Investigating Post-processing of Scanning Laser Ophthalmoscope Images for Unsupervised Retinal Blood Vessel Detection

Gavin Robertson[1]
gavin.robertson@ed.ac.uk

Enrico Pellegrini[2]
e.z.pellegrini@dundee.ac.uk

Calum Gray[1]
calum.gray@ed.ac.uk

Emanuele Trucco[2]
manueltrucco@computing.dundee.ac.uk

Tom MacGillivray[1]
t.j.macgillivray@ed.ac.uk

[1]*Clinical Research Imaging Centre, University of Edinburgh,* [2]*School of Computing, University of Dundee*

Abstract

We explore post-processing of scanning laser ophthalmoscope (SLO) images for the automatic detection of retinal blood vessels. The retinal vasculature is first enhanced using morphological and Gaussian matched filters before a thresholding technique produces a binary vessel map. Such permutations of post-processing techniques are commonly used to achieve unsupervised classification of the vasculature in fundus images, and it is the purpose of this study to investigate their applicability to SLO imaging. We compare the results of vascular detection as performed on SLO and fundus images.

1. Introduction

An image of the human retina reveals, among other structures, the branching of blood vessels radiating from the optic nerve head. This offers an exciting view of the body's microcirculation, without the need for an invasive procedure. Images can be captured quickly and safely without risk to the patient. There is increasing evidence that features associated with retinal blood vessels are early biomarkers of disease such as hypertension, stroke, and cardiovascular disease [1–4].

Modern devices such as the *fundus camera* and the *scanning laser ophthalmoscope* (SLO) allow images of the retina to be captured quickly and easily. In addition to the advances in image capture, the methods of analysis have progressed significantly.

Morphological processing [5–7] and Gaussian matched filtering [8] techniques are examples of commonly used methods of enhancing the retinal vasculature in fundus images prior to pixel classification to produce a binary vessel map. The focus of this preliminary study has been on the applicability of such techniques to SLO imaging that yield a much wider field of view (FoV) than fundus cameras (200° compared to 30°-60°) but which is far less well researched. We also focus on post-processing suited to unsupervised classification due to the time consuming task of producing training data sets for supervised learning techniques, especially considering the large FoV of SLO images.

The paper is arranged as follows. Section 2 details the source of the images used in this study. Section 3 details the vascular segmentation approach applied to the retinal images. The results are presented in Section 4 and, finally, Section 5 has some concluding remarks.

2. Materials

Wide-field retinal images were acquired using an Optos P200C SLO with a 200° FoV. For this pilot study a single SLO image (3900×3072 pixels) was hand segmented by a trained observer to produce a reference vessel map to compare against the results of computational segmentation.

The SLO is a fundamentally different technology to conventional fundus cameras that use a bright flash to illuminate the retina. Instead, a SLO uses low power laser light to raster scan the retina and sub-retinal layers to build up an image on a point-by-point basis. The Optos P200C SLO uses two laser sources, a green laser operating at 532nm and a red laser operating at 633nm to capture detail of the central retinal vasculature as well as detail of the more peripheral vessels.

For the purpose of vessel detection, the green channel image was chosen due to the superior contrast of the vasculature with respect to the retinal

978-1-4799-1053-3/13/$31.00

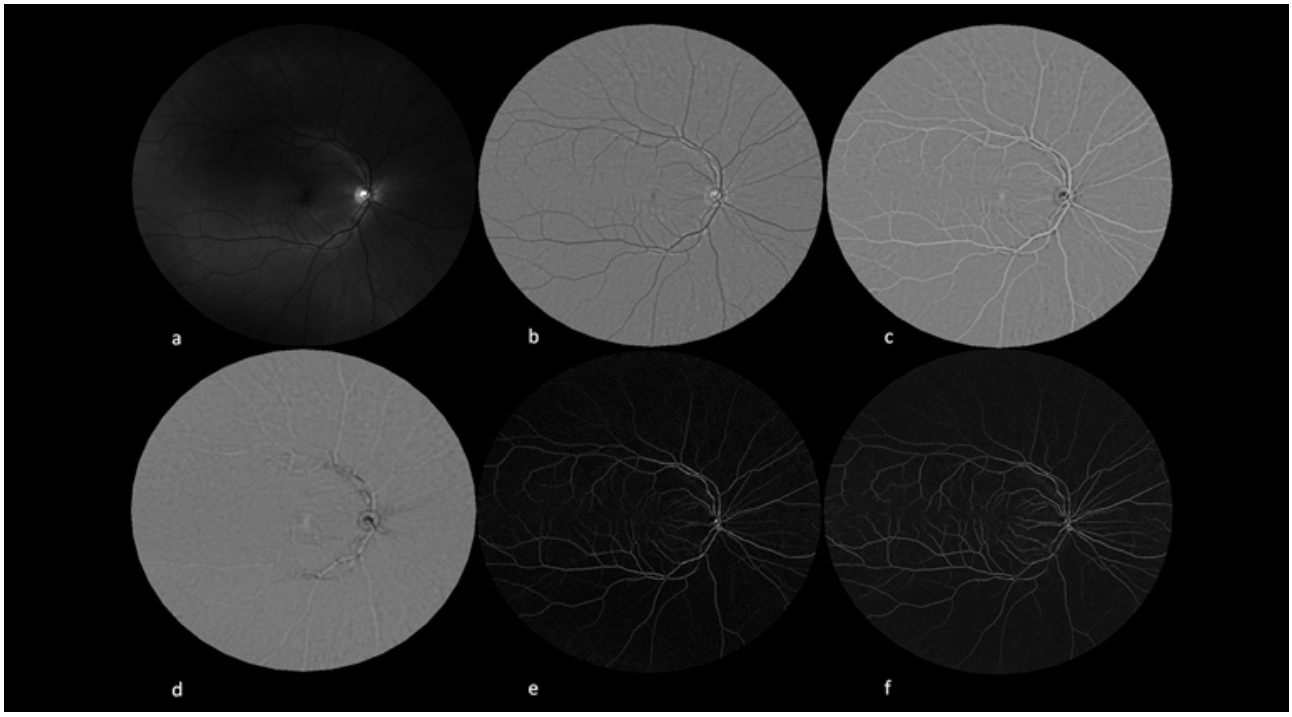

Figure 1. Vessel enhancement in SLO imaging. a – unprocessed green channel. b – median-based correction applied to input image to adjust for non-uniform illumination. c – maximum response to the morphological opening filter. d – minimum response to the morphological opening filter. e – result of morphological processing. f – result of Gaussian-based filtering to further enhance the vessels.

background. See Figure 1a.

Fundus images were acquired using a Canon CR-DGi nonmydriatic camera with a 45° FoV. 10 retinal images (876×584 pixels) were hand segmented by a trained observer to produce reference vessel maps. The size and width of vessels in the fundus and SLO are comparable, with a representative vessel width of approximately 10-20 pixels.

3. Methods

The proposed segmentation approach was based on exploiting the piece-wise linear appearance of the retinal vasculature and the typical Gaussian nature of the cross-sectional intensity profile of vessels. Lastly, the enhanced image undergoes a hysteresis thresholding step to create a binary vessel map.

A retinal image (regardless of the originating modality) was first processed to produce a padded border around the region-of-interest (ROI), i.e. the FoV boundary. This reduces unwanted effects at the step border between the ROI and the black background outside the FoV. The padded image was also inverted so that vessels appear lighter than the background. Next a morphological opening operation was performed on the image using a linear structuring element with dimensions 1×15 pixels. This length of neighbourhood was selected due to the typical widths of vessel as they appear in both SLO and fundus images. Morphological opening consists of an erosion followed by a dilation [9] and was repeated several times on the image with the structuring element rotated at 15° intervals. This was to account for vessels at various orientations. From the opened images the maximum response at each pixel location was selected to produce the output,

$$im_{\max} = \max_{i=0,\ldots,12}\left(im \circ st_i\right) \qquad (1)$$

where im is the original image, st_i is the structuring element at rotation i (0°, 15°, 30°, … 165°) and $im \circ st_i$ represents morphological opening. Morphological greyscale reconstruction [10] was performed to recover some small details lost in the previous step using the maximum response as the *marker* image and the inverted green channel as the *mask*.

The minimum response at each pixel location from the bank of opened images was also used to generate an image with vessels removed and to indicate local background intensity variations (Figure 1d). This was subtracted from the reconstructed image to produce an image where the vessels have been highlighted and the background suppressed (Figure 1e).

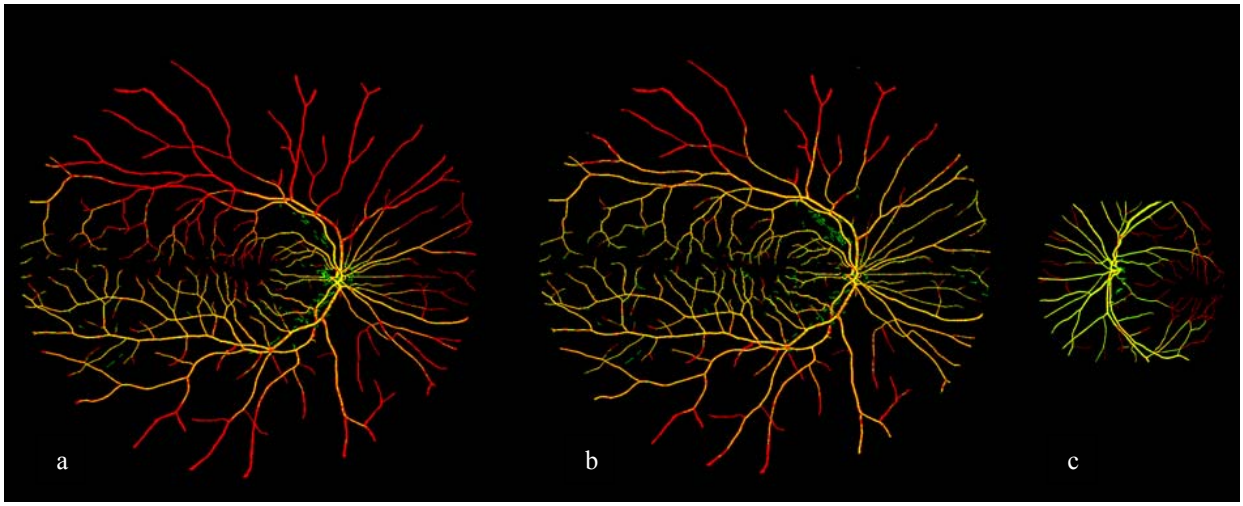

Figure 2. Assessing computational segmentation. a – background illumination uncorrected result, b - background illumination corrected result, and c - fundus result. False positives (green), false negatives (red), and vessel pixels successfully classified (yellow).

Further vessel enhancement was achieved with matched filtering using a combination of a Gaussian and Laplacian-of-Gaussian (LOG) filters [5]. The Gaussian filter (with σ of 1.75) was used to achieve smoothing of vessels along their directions, while the LOG filter, enhanced their contrast through a convolution step. Again, the filters were rotated in steps of 15º to account for different vessel orientations. The maximum pixel value at each pixel location was obtained, and the resultant output taken forward for further processing.

An additional morphological opening operation with a linear structuring element was performed to remove unwanted non-linear objects introduced by the Gaussian-based filtering, and a morphological greyscale reconstruction by erosion with 8-bit connectivity was performed to fill in holes and dark areas in the vessels (Figure 1f).

Equivalent processing steps were performed on the fundus images.

Finally, Hysteresis thresholding [5] was applied to produce a binary vessel map. Hysteresis thresholding introduces a second threshold level, so that there is an upper and lower bound. Any pixel value above the upper bound is set to 1, as are any pixels below the lower bound which are connected to (i.e. adjoining) pixels above the upper bound. Isolated pixels above the lower bound are set to 0. This helps to include dark vessels that are connected to lighter ones in a way absent from normal thresholding.

3.1. Background correction

A median-based filtering technique [11] was used as a pre-processing step for SLO imaging to correct for the substantial observed variance in background illumination (see Figure 1a) prior to the processing for vessel detection. A 50×50 pixel median filter was applied to the green channel image to create a map of the background illumination with vessels removed. By dividing the maximum value in this map by each pixel value, a 2D array of correction coefficients was created. This was multiplied with the original green channel and the subsequent intensity histogram profile adjusted to the middle of the available data range (i.e. 0 to 255 for an 8-bit image) to generate a corrected image (see Figure 1b).

4. Results and Discussion

After thresholding, the binary vessel maps were compared to the corresponding hand segmented maps in order to assess performance of computational vessel detection. The binary vessel maps were analysed with some well-known performance metrics for retinal vessel segmentation [12]. See Table 1.

The average performance of the computational segmentation on 10 fundus images is given in Table 2. The computational segmentation had a *TPR* (and standard deviation, SD) of 68.5% (5.2%), and *FPR* of 1% (0.2%). The overall accuracy of the segmentation for fundus images was 95.6% (0.6%).

The analysis was repeated for the SLO image, with assessment of the resulting vessel maps for both the uncorrected and background corrected. See Figure 2 for the graphical results. The median-based correction method improved the performance, especially in darker areas. The *TPR* increased from 34.6% to 54.6% (Table 2) though we note that this result is based on a preliminary investigation with only one SLO image

and that future investigation is intended on a larger number of SLO images.

Table 1. Performance metrics for retinal vessel segmentation.

Measure	Description
TP, FP, TN, FN	True Positive, False Positive, True Negative, False Negative.
True Positive Rate (TPR)	TP/vessel pixel count
False Positive Rate (FPR)	FP/non-vessel pixel count
Accuracy (Acc)	(TP+TN)/FoV pixel count

Further work is required to establish a more conclusive assessment of the performance of the vessel detection in SLO images by expanding the test data set. There is also scope for improving matched filtering by looking closely at the vessel properties in the two imaging modalities as well as more sophisticated thresholding and classification steps.

Table 2. Segmentation accuracy.

Fundus	TPR	FPR	Acc
Average	0.685	0.01	0.956
(SD)	(0.052)	(0.002)	(0.006)
SLO			
Original	0.346	0.002	0.942
Illumination corrected	0.546	0.003	0.957

5. Conclusion

The applicability of methods commonly employed for segmenting the retinal vasculature in fundus images has been explored for SLO imaging. We have demonstrated that such post-processing methods have huge scope for detecting the vasculature in SLO images, though more work is required to fully explore the performance with the expansion of the test data set.

6. Acknowledgements

This work was supported the Scottish Funding Council through the SINAPSE collaboration (www.sinapse.ac.uk). VAMPIRE software tools used here were made available by the VAMPIRE group at the Universities of Dundee and Edinburgh, UK (vampire.computing.dundee.ac.uk).

7. References

[1] F. N. Doubal, T. J. MacGillivray, et al, "Differences in retinal vessels support a distinct vasculopathy causing lacunar stroke", *Neurology*, May 2009., vol. 72, no. 20, pp. 1773–8.

[2] F. N. Doubal, P. E. Hokke, and J. M. Wardlaw, "Retinal microvascular abnormalities and stroke: a systematic review", *Journal of Neurology, Neurosurgery, and Psychiatry*, Feb. 2009, vol. 80, no. 2, pp. 158–65.

[3] N. Patton, T. M. Aslam, et al, "Retinal image analysis: Concepts, applications and potential", *Progress in Retinal and Eye Research*, Jan. 2006, vol. 25, no. 1, pp. 99–127.

[4] B. R. McClintic, J. I. McClintic, et al, "The Relationship between Retinal Microvascular Abnormalities and Coronary Heart Disease: A Review", *The American journal of medicine*, Apr. 2010, vol. 123, no. 4, pp. 374.

[5] C. Heneghan, J. Flynn, et al, "Characterization of changes in blood vessel width and tortuosity in retinopathy of prematurity using image analysis", *Medical Image Analysis*, Dec. 2002, vol. 6, no. 4, pp. 407–29.

[6] F. Zana and J. C. Klein, "Segmentation of vessel-like patterns using mathematical morphology and curvature evaluation", *IEEE Transactions on Image Processing*, Jul. 2001, vol. 10, no. 7, pp. 1010–9.

[7] A. M. Mendonça and A. Campilho, "Segmentation of retinal blood vessels by combining the detection of centerlines and morphological reconstruction", *IEEE Transactions on Medical Imaging*, Sep. 2006, vol. 25, no. 9, pp. 1200–13.

[8] S. Chaudhuri, S. Chatterjee, et al, "Detection of blood vessels in retinal images using two-dimensional matched filters," *IEEE Transactions on Medical Imaging*,Sep. 1989, vol. 8, no. 3, pp. 263–9.

[9] R. C. Gonzales and R. E. Woods, *Digital Image Processing*, Second Edi. Prentice-Hall, 2001.

[10] L. Vincent, "Morphological Grayscale Reconstruction in Image Analysis: Applications and Efficient Algorithms", *IEEE Transactions on Image Processing*, Apr. 1993, vol. 2, no. 2, pp. 176–201.

[11] R. Chrástek, M. Wolf, et al, "Automated segmentation of the optic nerve head for diagnosis of glaucoma", *Medical Image Analysis*, Aug. 2005, vol. 9, no. 4, pp. 297–314.

[12] M.M. Fraz, P. Remagnino, et al, "Blood vessel segmentation methodologies in retinal images – A survey", *Computer Methods and Programs in Biomedicine*, Aug. 2012, vol. 108, no. 1, pp. 407–433.